Available online at www.sciencedirect.com
SCIENCE DIRECT®
Vision Research 46 (2006) 869–878
Vision Research
www.elsevier.com/locate/visres

The visual motion detectors underlying ocular following responses in monkeys

Kenichiro Miura [a,b,*], Kiyoto Matsuura [b], Masakatsu Taki [b,c], Hiromitsu Tabata [a,b], Naoko Inaba [b], Kenji Kawano [b], Frederick A. Miles [d]

[a] *Horizontal Medical Research Organization, Graduate School of Medicine, Kyoto University, Japan*
[b] *Department of Integrative Brain Science, Graduate School of Medicine, Kyoto University, Japan*
[c] *Department of Otolaryngology, Kyoto Prefectural University of Medicine, Japan*
[d] *Laboratory of Sensorimotor Research, National Eye Institute, National Institutes of Health, USA*

Received 8 August 2005; received in revised form 20 October 2005

Abstract

Psychophysical evidence indicates that visual motion can be sensed by low-level (energy-based) and high-level (feature-based) mechanisms. The present experiments were undertaken to determine which of these mechanisms mediates the initial ocular following response (OFR) that can be elicited at ultra-short latencies by sudden motion of large-field images. We used the methodology of Sheliga, Chen, Fitzgibbon, and Miles (Initial ocular following in humans: A response to first-order motion energy. *Vision Research*, 2005a), who studied the initial OFRs of humans, to study the initial OFRs of monkeys. Accordingly, we applied horizontal motion to: (1) vertical square-wave gratings lacking the fundamental (''missing fundamental stimulus'') and (2) vertical grating patterns consisting of the sum of two sinusoids of frequency 3*f* and 4*f*, which created a repeating pattern with beat frequency, *f*. Both visual stimuli share a critical property: when subject to 1/4-wavelength steps, their overall pattern (feature) shifts in the direction of the steps, whereas their major Fourier component shifts in the reverse direction (because of spatial aliasing). We found that the initial OFRs of monkeys to these stimuli, like those of humans, were always in the opposite direction to the 1/4-wavelength shifts, i.e., in the direction of the major Fourier component, consistent with detection by (low-level) oriented spatio-temporal filters as in the well-known energy model of motion analysis. Our data indicate that the motion detectors mediating the initial OFR have quantitatively similar properties in monkeys and humans, suggesting that monkeys provide a good animal model for the human OFR.

Keywords: Missing fundamental; Spatio-temporal filtering; Energy-based mechanisms; Eye movements

1. Introduction

In primates, sudden movements of the visual scene elicit ocular following responses (OFRs) with ultra-short latencies: <80 ms in humans and <60 ms in monkeys with some stimuli (Gellman, Carl, & Miles, 1990; Miles, Kawano, & Optican, 1986; Sheliga et al., 2005a, 2005b). It is believed that OFRs assist in the rapid stabilization of gaze with respect to the (stationary) surroundings (Miles, 1998), and there is substantial evidence that, in monkeys, it is mediated in large part by cortical area MST (Kawano, Inoue, Takemura, Kodaka, & Miles, 2000; Kawano, Shidara, Watanabe, & Yamane, 1994; Takemura, Inoue, & Kawano, 2002). Because the OFR is driven by retinal image motion, it has recently been used to study some of the neural processes underlying the sensing of visual motion in humans (Chen, Sheliga, Fitzgibbon, & Miles, 2005; Masson, Busettini, Yang, & Miles, 2001; Masson & Castet, 2002; Masson, Yang, &

* Corresponding author. Tel.: +81 75 753 4485; fax: +81 75 753 4486.
E-mail address: kmiura@brain.med.kyoto-u.ac.jp (K. Miura).

0042-6989/$ - see front matter © 2005 Elsevier Ltd. All rights reserved.
doi:10.1016/j.visres.2005.10.021

Miles, 2002; Sheliga et al., 2005a; Sheliga, Chen, Fitzgibbon, & Miles, 2005b; Yang & Miles, 2003). It is generally believed that there are at least two different neural mechanisms by which we analyze visual motion, and various descriptors have been applied to them, based in part on the methodology that was used to investigate them: see Lu and Sperling (2001) for review. One mechanism utilizes low-level visual motion detectors that are sensitive to luminance modulation, and functions without regard for form or features. This mechanism is variously referred to as, 1st-order, Fourier or energy-based. The other, high-level, mechanism(s) extracts visual motion using features to which the low-level visual motion detectors are insensitive, and is referred to as 2nd-order, non-Fourier or feature-based. We will use these various terms interchangeably, although they are not strictly synonymous.

Using special broad-band stimuli, Sheliga et al. (2005a, 2005b) recently demonstrated that the initial OFR in humans is largely determined by the motion of the principal Fourier component of the visual stimulus, as though reliant on oriented spatio-temporal visual filters as in the well-known energy model of motion detection, i.e., the human OFR is mediated by low-level motion detectors. These workers elicited OFRs with two kinds of apparent-motion stimuli whose features and principal Fourier components moved in opposite directions under the assumption that the brain gives the greatest weight to the nearest-neighbor matches (Georgeson & Harris, 1990; Hammett, Ledgeway, & Smith, 1993; see also Pantle & Turano, 1992). One was the missing fundamental (*mf*) stimulus, which can be constructed from a square wave by subtracting the fundamental sine-wave component. In the frequency domain, the *mf* stimulus consists of summed odd harmonics, the largest being the 3rd and the remainder having progressively decreasing amplitudes such that the *i*th harmonic has an amplitude proportional to $1/i$. Sheliga et al. (2005a, 2005b) moved the *mf* stimulus in discrete 1/4-wavelength steps rather than smoothly because, when so moved, all of its harmonics are shifted 1/4 of their wavelengths, the $4n+1$ harmonics (where n is an integer) shifting in the direction of the actual image shifts (i.e., forwards, along with the entire pattern and its features), whereas the $4n-1$ harmonics (which include the principal Fourier component, the 3rd harmonic) shift in the opposite direction (i.e., backwards). Notice that a 3/4-wavelength forward shift of a pure sine-wave is exactly equivalent to a 1/4-wavelength backward shift because of spatial aliasing, and it is invariably the latter that determines the direction of any associated OFRs and perceived motion (Pantle & Turano, 1992). The other apparent-motion stimulus used by Sheliga et al. was the so-called 3*f*4*f* stimulus, which is a repeating pattern with a spatial-frequency of f that is constructed by summing two sinusoids of equal-amplitude whose spatial frequencies are in the ratio 3:4, the 3*f* and 4*f* components (Hammett et al., 1993). When this pattern is shifted forwards in successive steps that are each 1/4 of the wavelength of the beat, the 4*f* component is effectively stationary while the 3*f* component steps backward 1/4 of its wavelength because of spatial aliasing, exactly as with the $4n-1$ harmonics of the *mf* stimulus. Sheliga et al. (2005a, 2005b) reported that the initial OFRs elicited by these *mf* and 3*f*4*f* stimuli in humans were invariably in the direction of motion of their principal Fourier component(s) rather than the direction of motion of their features, consistent with a mechanism that has oriented spatio-temporal filters and senses 1st-order motion (cf., Masson et al., 2002). Indeed, Sheliga et al. (2005a) have suggested that the initial OFR of humans provides a model system for studying neural sensors that respond selectively to 1st-order visual motion and do not respond to 2nd-order motion. Psychophysical studies indicate that when 1/4-wavelength steps are applied to *mf* stimuli human observers generally—but not always—perceive them to move in the opposite direction to their true motion (Adelson, 1982; Adelson & Bergen, 1985; Baro & Levinson, 1988; Brown & He, 2000; Georgeson & Harris, 1990; Georgeson & Shackleton, 1989). Also, human observers generally experience motion transparency when viewing 3*f*4*f* stimuli, seeing rapid forward motion of the beat and slower reverse motion of the 3*f* component, consistent with the simultaneous activation of feature-based (2nd-order) and energy-based (1st-order) sensing mechanisms, respectively (Hammett et al., 1993).

To further examine the neural mechanisms underlying the visual motion detectors underlying initial OFRs, it is critical to have an adequate animal model. We were interested in the monkey as one such model but were concerned by a previous report, based on one monkey, which concluded that the initial OFRs to motion defined by contrast modulated noise—a pure 2nd-order motion stimulus—were essentially the same as to motion defined by luminance modulations—1st-order motion—except for a very slight difference in latency (Benson & Guo, 1999). Further, there have been a number of reports that some neurons in the middle temporal area (MT) of the monkey are sensitive to 2nd-order motion (Albright, 1992; Ilg & Churan, 2004; O'Keefe & Movshon, 1998). We now report that the initial OFRs elicited in macaque monkeys when 1/4-wavelength steps are applied to *mf* and 3*f*4*f* stimuli are in all essentials like those described by Sheliga et al. (2005a) in humans—being dominated in large part by the 1st-order motion energy in the principal Fourier components—indicating that the monkey is a good animal model.

2. Methods

Data were collected from two rhesus monkeys (*Macaca fuscata*), weighing 7.7 (A) and 8.8 kg (B). All procedures reported here were approved by the Institute's Animal Care and Use Committee. Many of the general procedures were the same as those used in previous studies of ocular tracking in monkeys (Kawano et al., 1994; Kodaka, Miura, Suehiro, Takemura, & Kawano, 2004) and humans (Sheliga et al., 2005a) and so will only be given in brief.

2.1. Animal preparations

The monkeys were previously trained to fixate a small spot. Under pentobarbital sodium anesthesia and aseptic conditions, each monkey was implanted with a head holder, which allowed the head to be fixed in the standard stereotaxic position during the experiments, and a scleral search coil to allow measurement of the position of the right eye (Judge, Richmond, & Chu, 1980).

2.2. Visual display and stimuli

The animals faced a 19 in CRT monitor (Eizo T766, driven by a PC Radeon 9800 Pro video card), which was 50 cm in front of the eyes, in a dark room. Visual stimuli were presented on the monitor (resolution, 1280 × 1024 pixels; vertical refresh rate, 100 Hz). The RGB signals from the video card were converted to black and white images with 11-bit grayscale resolution through an attenuator (Pelli, 1997), exactly as described by Sheliga et al. (2005a). Briefly, a luminance look-up table with 256 equally spaced luminance levels ranging from 0.3 to 77.1 cd/m^2 was created by direct luminance measurements (LS-100 photometer; Konica-Minolta, Japan) under software control. This table was then expanded to 2048 equally spaced levels by interpolation.

The visual images consisted of one-dimensional vertical grating patterns that could have one of four horizontal luminance profiles in any given trial: (1) a square wave with a missing fundamental (*mf* stimulus), achieved by summing the odd harmonics (starting with the 3rd harmonic and finishing with the highest harmonic that fell short of the Nyquist frequency) as described by Sheliga et al. (2005a); (2) a sum of two equal-amplitude sinusoids whose spatial frequencies were in the ratio 3:4 (3*f*4*f* stimulus); (3) a pure sine-wave with the same frequency as the beat of the *mf* and 3*f*4*f* stimuli (1*f* stimulus); (4) a pure sine-wave whose spatial frequency was three times that of the 1*f* stimulus (3*f* stimulus), and hence was the same as that of the principal Fourier component of the *mf* stimulus (the 3rd harmonic) and the 3*f* component of the 3*f*4*f* stimulus. Each image extended 360 mm horizontally (39.6°; 1280 pixels) and 270 mm vertically (30.2°; 1024 pixels) and had a mean luminance of 38.7 cd/m^2. The initial phase of a given grating was randomized from trial to trial at intervals of 1/4-wavelength. Motion was created by substituting a new image every frame (i.e., every 10 ms) for a total of 15 frames (i.e., stimulus duration, 150 ms), each new image being identical to the previous one except phase shifted horizontally by 1/4 of the wavelength of the fundamental. In any given trial the successive steps were all in the same direction (rightward or leftward, randomly selected). We examined the OFRs elicited by these apparent-motion stimuli at various stimulus contrast levels (1, 2, 4, 8, 16, 32, and 64%, where the contrast was defined as, $((L_{max} - L_{min})/(L_{max} + L_{min}))*100\%$, L_{max}, and L_{min} being the maximum and minimum luminance levels, respectively). An experimental block consisted of 56 stimulus entries (4 grating patterns, 2 directions of motion, and 7 contrast levels), all of which were interleaved and randomly ordered in individual blocks.

2.3. Procedures

At the beginning of each trial, a grating pattern appeared together with a central target spot (diameter, 0.4°) that the animal had been trained to fixate. After the monkey's right eye had been positioned within 2° of the fixation target for a randomized period of 750–1000 ms (and no saccades had been detected for the last 250 ms in this period), the fixation target disappeared and the apparent-motion stimulus began. Otherwise, the screen became uniform gray and the trial was repeated. The motion lasted for 150 ms, at which time the screen became a uniform gray with the same mean luminance. Then, the animals were rewarded with a drop of juice, signaling the end of the trial. After an inter-trial interval of 1000–1500 ms, a new grating pattern appeared together with a fixation point, commencing a new trial. Data were collected over several sessions until each condition had been repeated an adequate number of times to permit good resolution of the responses through averaging.

2.4. Data collection and analyses

All aspects of the experimental paradigms were controlled by two PCs, which communicated via Ethernet using the TCP/IP protocol. One of the PCs was running a Real-time EXperimentation software package (REX) developed by Hays, Richmond, and Optican (1982), and provided the overall control of the experimental protocol as well as acquiring, displaying, and storing the eye-movement data. The other PC was running Matlab subroutines, utilizing the Psychophysics Toolbox extensions (Brainard, 1997; Pelli, 1997), and generated the visual stimuli upon receiving a start signal from the REX machine.

Eye movements were measured using the electromagnetic search coil technique (Fuchs & Robinson, 1966). The voltage signals encoding the horizontal and vertical components of the eye position were passed through an analog low-pass filter (−3 dB at 200 Hz) and were digitized to a resolution of 12 bits, sampling at 1 kHz. All data were stored and transferred to another PC for analysis using computer programs based on Matlab (The Mathworks). The eye-position data were smoothed with a 3-pole digital butterworth filter (−3 dB at 30 Hz), and eye-velocity traces were derived from the two-point backward difference. Eye acceleration profiles were derived from the two-point backward difference of the eye-velocity traces, and were used to detect small saccades that went undetected during the experiment. Trials with saccadic intrusions were then discarded (on average, 23% in monkey A and 27% in monkey B). Mean temporal eye-velocity profiles were computed for each of the stimulus

conditions. To obtain low-noise estimates of eye-velocity, responses were averaged over at least 31 trials in the preliminary experiment on spatial-frequency and 40 trials in the main experiment on contrast.

The initial horizontal OFRs were quantified by measuring the changes in horizontal eye position over the 50-ms time periods starting 50 ms after the onset of the motion stimuli. The minimum latency of onset was ~50 ms so that these response measures were restricted to the period prior to the closure of the visual feedback loop (i.e., twice the reaction time): initial open-loop responses. The responses to rightward and leftward were pooled to improve the signal-to-noise ratio by subtracting the mean response to a given leftward motion stimulus from the mean response to the corresponding rightward motion stimulus, and these will be referred to the "R–L responses." The 95% confidence intervals were calculated to indicate the extent of the fluctuations in R–L measures. Because rightward eye movements were positive in our sign convention, these pooled R–L measures were positive when the OFR was in the direction of the applied image shift (also sometimes referred to as the "forward" direction, in contradistinction to the "backward" or "reverse" direction).

3. Results

3.1. Dependence on spatial-frequency

To determine what spatial-frequency to use for the *mf* and 3*f*4*f* stimuli, we did a preliminary experiment in which we applied 1/4-wavelength steps to pure sinusoidal vertical gratings (contrast, 32%) with a wide range of spatial frequencies (0.05, 0.10, 0.20, 0.40, 0.81, and 1.62 cycles/°). Fig. 1 shows the data obtained from both monkeys, with the mean R–L velocity traces over time above (A and C) and the associated mean R–L change-in-position measures plotted against spatial-frequency below (B and D). All OFRs were in the forward direction, which is positive in our convention (see Methods) and so they are rendered as upward deflections of the R–L velocity traces (from a zero baseline) in Figs. 1A and C. The R–L measures displayed clear band-pass dependence on spatial-frequency that was well-represented by Gaussian functions (r^2 values: 0.995, 0.996) with peaks (f_o) at 0.158, and 0.291 cycles/°

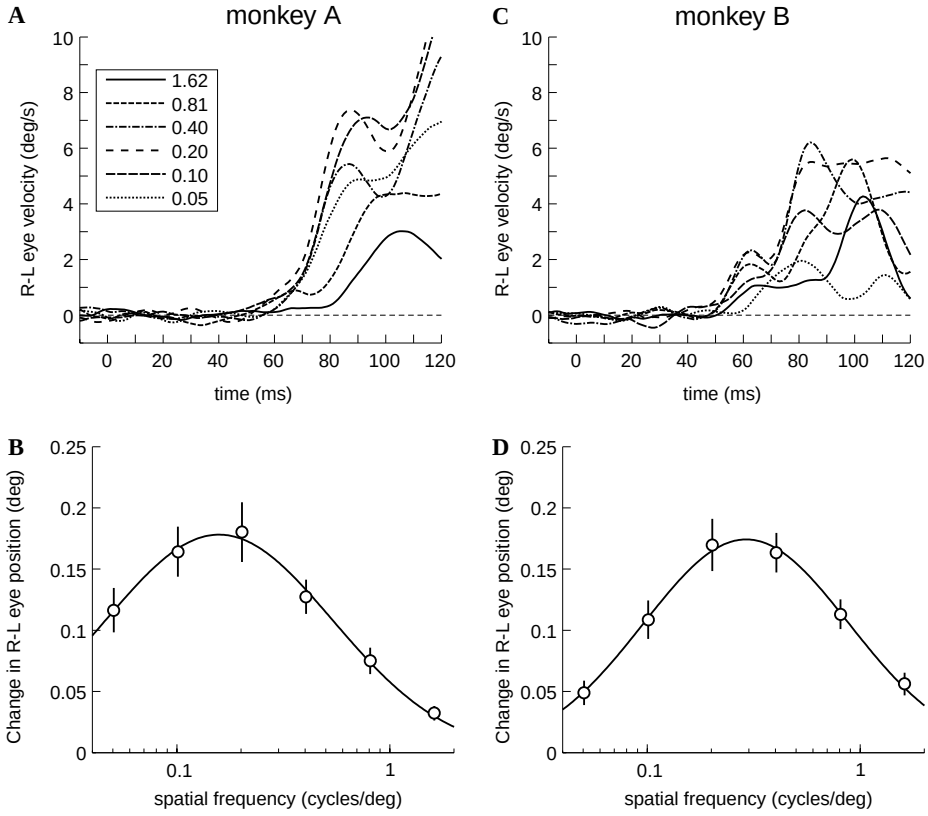

Fig. 1. The initial OFR elicited by 1/4-wavelength steps applied to sinusoidal grating patterns (1*f* stimulus): dependence on spatial-frequency (two monkeys). (A and C) Mean R–L eye-velocity temporal profiles: see key for spatial frequencies (in cycles/°). Upward deflections of the traces from the zero baseline (dashed horizontal line) denote forward motion (in the direction of the steps). Zero on the abscissa denotes the time of the first 1/4-wavelength shift (defined as the onset of stimulus motion). (B and D) Mean R–L response measures (mean change in R–L position during the time period 50–100 ms after the onset of motion) plotted as a function of the spatial-frequency in cycles/°; note that the abscissa has a logarithmic scale. The smooth curves are the best fit Gaussian functions: see Sheliga et al. (2005a) for methods. The data for monkey A are in (A and B) (31–37 trials per condition; SD's ranged 0.018–0.072°) and the data for monkey B are in (C and D) (59–73 trials per condition; SD's ranged 0.039–0.089°). Contrast, 32%. Error bars, 95% confidence intervals.

and standard deviations (σ) of 0.534 and 0.482 log units in monkey A and monkey B, respectively: see the continuous smooth curves in Figs. 1B and D and note the logarithmic abscissas. These parameters of the fitted Gaussian functions were used to derive a low-frequency cutoff (f_{lo}) and a high-frequency cutoff (f_{hi}), defined as the spatial frequencies at which the tuning curve was half its maximum, using the following expression from Read and Cumming (2003): $f_o \exp(\pm\sigma\sqrt{\ln 4})$. The computed values of f_{lo} were 0.037, and 0.079 cycles/°, and the computed values of f_{hi} were 0.672, and 1.077 cycles/°. The initial OFRs of humans show a very similar Gaussian dependence on log spatial-frequency (Sheliga et al., 2005a). Based on these findings, the fundamental spatial frequencies (*f*) selected for the *mf* and 3*f*4*f* stimuli were 0.09 cycles/° for monkey A and 0.15 cycles/° for monkey B, thereby ensuring that the initial OFRs elicited by pure sine-waves of spatial-frequency 1*f* and 3*f* were of similar amplitude.

3.2. Dependence on contrast

Fig. 2 shows the mean OFR temporal profiles (again, R–L responses) elicited from monkey A by successive discrete phase shifts applied to each of the four different grating patterns over a wide range of contrasts. The shifts always had the same absolute amplitude, 2.78°, which meant that with each shift the 1*f*, *mf*, and 3*f*4*f* gratings stepped forwards 1/4 of their wavelength (given that their wavelengths were all 11.1°), whereas the 3*f* grating stepped forwards 3/4 of its wavelength, which was equivalent to a *backward* step of 1/4 of its wavelength. Let us first consider the data obtained with the pure sine-wave stimuli. It is evident from Fig. 2 that the initial OFRs elicited by the 1*f* stimulus were always in the *forward* direction whereas those elicited by the 3*f* stimulus were always in the *backward* direction, exactly in accord with the shortest-path or nearest-neighbor matches for these stimuli: spatial aliasing. Of course, a pure sine-wave has only one Fourier component and this always shifts together with its features (peaks and troughs), so it is not possible to determine which of these two attributes of the motion stimulus elicited the OFR here. Turning to the more complex grating patterns, however, it is evident that the initial OFR elicited by the *mf* and 3*f*4*f* stimuli were always in the *backward* direction, which was the direction of motion of their

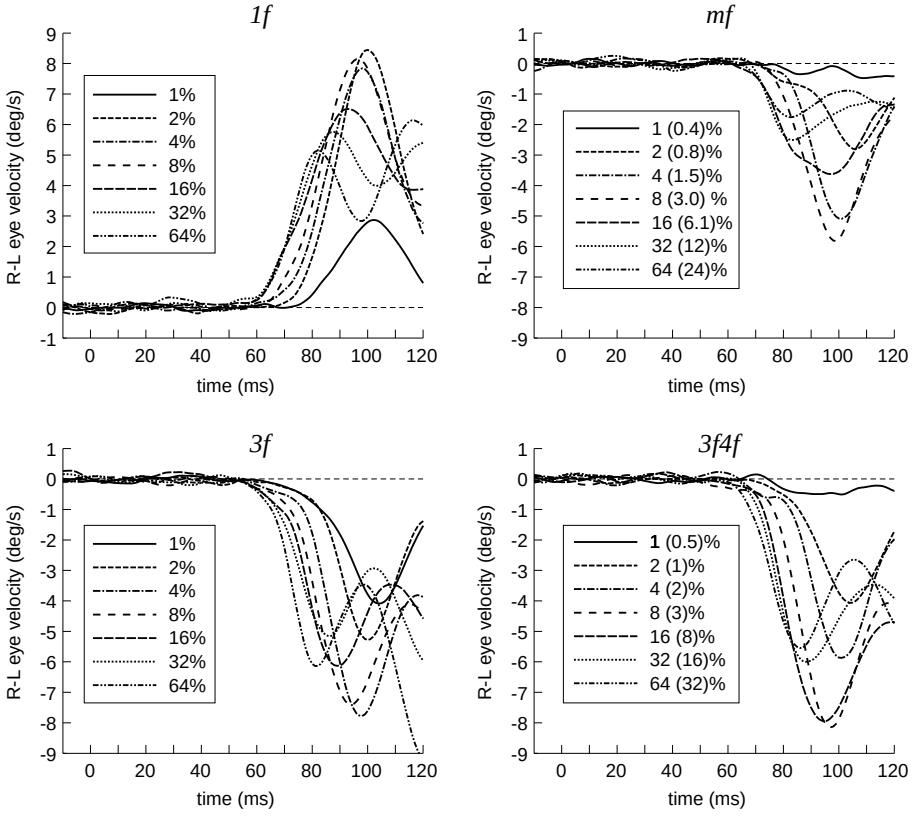

Fig. 2. The initial OFR: dependence on contrast (eye velocity traces from monkey A). All motion stimuli consisted of successive shifts that had the same absolute amplitude, 2.78°, which was 1/4 of the wavelength of the 1*f*, *mf*, and 3*f*4*f* gratings, whose fundamentals all had wavelengths of 11.1° (spatial frequencies, 0.09 cycles/°), and 3/4 of the wavelength of the 3*f* grating, whose wavelength was 3.7° (spatial-frequency, 0.27 cycles/°). Traces show the mean R–L eye-velocity temporal profiles. The keys indicate the contrasts, those values in parentheses for the *mf* and 3*f*4*f* data indicating the contrasts of the 3rd harmonic and 3*f* component, respectively. Upward deflections of the traces from the zero baselines (dashed horizontal lines) denote forward motion (in the direction of the steps). Abscissas denote the time from the first stimulus shift (defined as the onset of stimulus motion).

principal Fourier components (the 3rd harmonic and the 3*f* component, respectively) and opposite to the direction of motion of their features.

Let us scrutinize the response profiles in Fig. 2 more closely, starting with those obtained with the 1*f* stimulus (upper left). At the lowest contrast (1%), the initial transient OFR had a latency of 70–80 ms and reached a peak at ~100 ms after the onset of the apparent-motion (i.e., the time of the first step). As the stimulus contrast was increased to 2%, this initial transient showed a slight reduction in latency and a substantial increase in amplitude. Further increases in stimulus contrast resulted in shorter onset latencies with *reduced* initial peaks, which is the "anomalous contrast-dependence" originally described by Miles et al. (1986), who recorded the initial OFR elicited from monkeys when velocity steps were applied to pure sine-wave gratings. The response profiles obtained with the 3*f* stimulus (lower left in Fig. 2) show a similar general pattern even though of the opposite sign, as also do the profiles obtained with the *mf* stimulus (upper right in Fig. 2) and the 3*f*4*f* stimulus (lower right in Fig. 2), consistent with mediation largely by their 3*f* components. The profiles obtained with the *mf* stimulus, however, are clearly much lower in amplitude than those obtained with the other stimuli. The OFRs of the other monkey, which are not illustrated, showed the same general tendencies.

The anomalous reductions in the amplitude of the initial peak in the OFR profiles as contrast was increased beyond 2% were attributed by Miles et al. (1986) to a reduction in the time available to integrate the motion error signal because of the associated decreases in latency, and they successfully modeled this effect. Indeed, these workers also showed that no such anomalous dependence on contrast was apparent when the velocity responses were integrated over a fixed interval time-locked to motion onset and approximating the initial open-loop period, as though the reductions in velocity amplitude were offset by the reductions in the latency of response onset. We too found this same effect in our data and report it in Fig. 3, which shows the dependence on stimulus contrast of the initial OFR based on the changes in the mean R–L position measures over the time period 50–100 ms (measured from the time of the first step), for all four grating patterns and both monkeys. The R–L response measures for the data obtained with the 1*f* and 3*f* stimuli (filled and open circles in Fig. 3), generally showed a monotonic rise as the stimulus contrast increased, gradually saturating as contrast reached 5–10% in monkey A and 20–30% in monkey B (note the log abscissa). Of course, the 1*f* data all have positive values (being in the forward direction) and the 3*f* data all have negative values (being in the backward direction). These data were fitted with the following expression:

$$R_{\max}\frac{c^n}{c^n + c_{50}^n}, \tag{1}$$

where $R_{\max}$ is the maximum attainable response, c is the contrast, c_{50} is the semi-saturation contrast (at which the response has half its maximum value), and n is the exponent that sets the steepness of the curves.

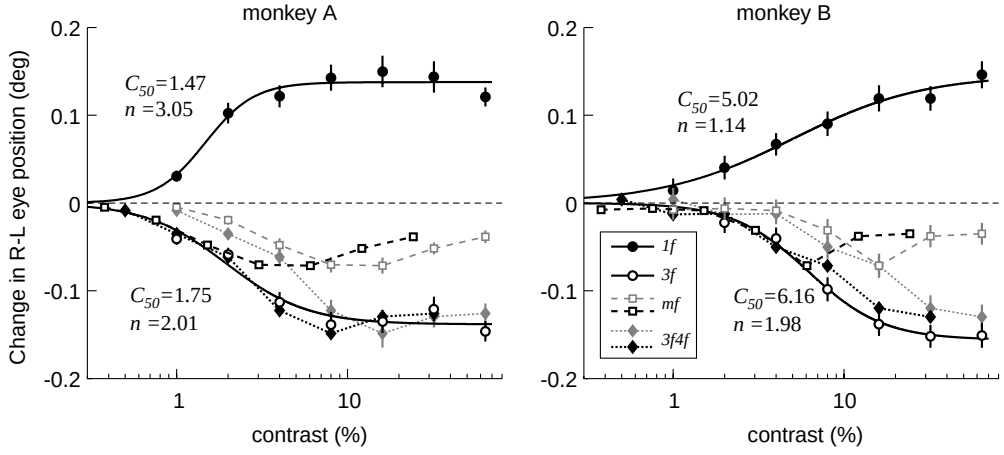

Fig. 3. The initial OFR: dependence on contrast (R–L response measures for two monkeys). Plots show the horizontal OFR elicited when successive steps (each 2.78° for monkey A and 1.67° for monkey B) were applied to *mf* and 3*f*4*f* stimuli (spatial frequencies and wavelengths: monkey A, 0.09 cycles/° and 11.1°; monkey B, 0.15 cycles/° and 6.67°) as well as to pure sine-wave gratings whose spatial frequencies matched the 1*f* or 3*f* components of the complex gratings. Responses to the pure 1*f* sine-waves (filled circles) were always positive (OFR in the forward direction), whereas those to the *mf* stimulus (gray open squares, gray dashed lines), the 3*f*4*f* stimulus (gray filled diamonds, gray dotted lines), and the pure 3*f* sine-waves (open circles) gratings were always negative (OFR in the backward direction). Responses to the *mf* and 3*f*4*f* gratings are also replotted as a function of the contrast of their 3*f* components to permit easy comparison with the pure 3*f* sine-wave data (*mf*, black open squares and dashed lines; 3*f*4*f*, black filled diamonds and dotted lines). The smooth black curves are best-fit Naka–Rushton functions for the pure sine-wave data and the values of their c_{50} and n parameters are shown nearby. Monkey A: 40–56 trials per condition; SD's ranged 0.017–0.062°. Monkey B: 40–54 trials per condition; SD's ranged 0.038–0.054°. Error bars, 95% confidence intervals.

This expression is based on the Naka–Rushton equation (Naka & Rushton, 1966) and provides a good fit to the contrast-dependence curves of neurons in the LGN, V1, and MT of monkeys (Albrecht, Geisler, Frazor, & Crane, 2002; Albrecht & Hamilton, 1982; Heuer & Britten, 2002; Sclar, Maunsell, & Lennie, 1990), as well as to the human contrast-dependence curves for the initial OFRs to moving sine-wave gratings (Sheliga et al., 2005a) and unikinetic plaid patterns (Masson & Castet, 2002). The continuous smooth curves in Fig. 3 are the best fit curves using this expression and are clearly good approximations to the data with r^2 values >0.9 for all curves. The values of c_{50} for the 1*f* and 3*f* stimuli were 1.47 and 2.01%, respectively, for monkey A, and 5.02 and 6.16%, respectively, for monkey B. The values of n for the 1*f* and 3*f* stimuli were 3.05 and 1.75, respectively, for monkey A, and 1.14 and 1.98, respectively, for monkey B. Thus, the OFRs were most sensitive to changes in contrast when the contrast was relatively low (<5% for monkey A and <20% for monkey B).

If the initial OFRs to the *mf* and 3*f*4*f* stimuli are actually generated by their principal Fourier components, the 3rd harmonic and the 3*f* component, respectively, then when plotted in terms of the contrast of these components, their contrast-dependence data should overlay those obtained with pure sine waves of the same spatial-frequency, i.e., the data obtained with the 3*f* stimulus. The data obtained with the *mf* stimulus (squares and dashed lines in Fig. 3) and the 3*f*4*f* stimulus (diamonds and dotted lines in Fig. 3) are therefore plotted as a function of both the actual contrast of the patterns (gray symbols and lines) and the contrast of their 3rd harmonic and 3*f* components (black symbols and lines). As we pointed out earlier, the OFRs to these *mf* and 3*f*4*f* stimuli were always in the opposite direction to the actual shifts of the patterns and so have negative values in Fig. 3. When plotted as a function of the contrast of their 3*f* component, the data obtained with the 3*f*4*f* stimulus approximated those obtained with the pure sine-wave 3*f* stimuli, though tending to fall a little short at higher contrasts in monkey B. When plotted as a function of the contrast of their 3rd harmonic, the data obtained with the *mf* stimulus also closely approximated those obtained with the 3*f* stimulus at low contrast (<3% for monkey A, <8% for monkey B), but fell substantially short of this with higher contrast stimuli. Very similar trends are seen in humans (Sheliga et al., 2005a).

For monkey A, the 3*f*4*f* data in Fig. 3 closely approximate the pure 3*f* data (when plotted as a function of the contrast of the 3*f* component), indicating that the 4*f* component of the 3*f*4*f* stimulus had almost no impact on the initial OFR measures, and this was also apparent from the R–L temporal response profiles: see Fig. 4 (left column) and compare the thick traces (the 3*f*4*f*-stimulus data) with the thin traces (the 3*f*-stimulus data). For monkey B, the 3*f*4*f*-stimulus data fell short of the 3*f*-stimulus data at high contrast and the R–L temporal profiles in Fig. 4 (right column) indicate that the impact of the 4*f* component was not uniform but rather selectively affected a small early transient component and a later sustained component (that was mostly outside the open-loop measurement period) and left the main body of the response profile largely intact.

4. Discussion

4.1. The monkey as a model for the human

Our data show that the initial OFRs of the monkey share many fundamental properties with those of the human recently described by Sheliga et al. (2005a, 2005b), indicating that the monkey provides an excellent animal model. The initial support for this conclusion comes from the data obtained with the pure sine-wave stimuli and these are further reinforced by the data obtained with the more complex *mf* and 3*f*4*f* stimuli. Let us start by comparing the quantitative R–L response measures obtained with pure sine-wave stimuli in the two studies. The initial OFRs of our monkeys and of Sheliga et al.'s humans showed a dependence on spatial-frequency that was clearly band-pass and well described by Gaussian functions (with a log abscissa). Even the parameters of the best-fit Gaussians were very similar in the two species. For example, mean values for the three humans in the Sheliga et al. study vs. mean values for our two monkeys were as follows: $f_o = 0.25$ vs 0.22 cycles/°; $\sigma = 0.51$ vs 0.51 log units; $f_{lo} = 0.06$ vs 0.06 cycles/°; $f_{hi} = 0.99$ vs 0.87 cycles/°. The dependence on contrast also had a very similar form in monkeys and humans, showing a smooth monotonic rise with saturation at moderate contrast levels that was well-fit by the Naka–Rushton equation, whose parameters were again quite similar in our two studies (even though the data from the two monkeys showed much more scatter than the data from the three humans). For example, the mean best-fit Naka–Rushton parameters for the 1*f* data (human vs monkey) were as follows: $c_{50} = 3.9$ vs 3.24%; $n = 2.10$ vs 2.09, and the equivalent 3*f* data are: c_{50}=5.7 vs 4.09%; $n = 1.55$ vs 1.87. Nonetheless, the anomalous dependency on contrast that is evident in the initial peak of the monkey's eye-velocity traces in both our study and that of Miles et al. (1986), whereby over part of the contrast range, *increases* in contrast were associated with *decreases* in the amplitude of the initial peak in eye-velocity, is not seen in the temporal profiles of the human OFR (Sheliga et al., 2005a). This anomaly presumably had no obvious impact on our integrated-velocity measures that were time-locked

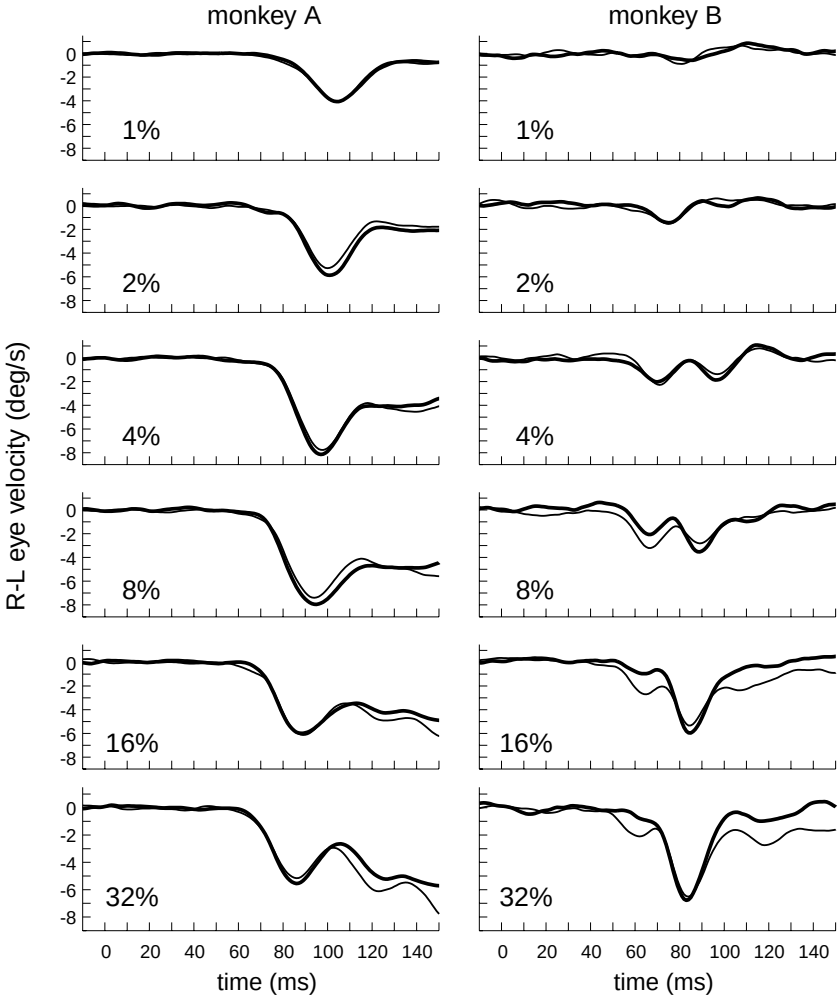

Fig. 4. Comparison of the OFRs elicited by 3*f* and 3*f*4*f* stimuli with a range of contrasts (temporal profiles for two monkeys). All shifts and wavelengths were as given in the legend of Fig. 3. Each panel shows the mean R–L temporal velocity profiles elicited by the 3*f* stimulus alone (thin line), and the 3*f*4*f* stimulus (thick line) whose 3*f* component had a contrast that matched that of the 3*f* stimulus and is listed on each plot (in %). All responses deflected the traces downward from the zero baseline, denoting backward eye movements (in the direction of the principal Fourier component). Abscissas denote the time from the first stimulus shift (defined as the onset of stimulus motion).

to stimulus onset (i.e., the change-in-position measures in Fig. 3) because of the associated latency changes, as originally pointed out by Miles et al. (1986). In fact, the latency of the monkey's OFR (to smoothly drifted sinusoidal gratings) is solely a function of contrast and temporal frequency (Miles et al., 1986), whereas the latency of the human's OFR is also somewhat sensitive to speed and spatial-frequency (Gellman et al., 1990) and less sensitive to contrast (see Fig. 5 of Sheliga et al., 2005a). However, these detailed differences in the latency and development of the very earliest OFRs of monkeys and humans ultimately have little consequence for the overall tracking responses as indicated by the similarity of their integrated-velocity measures over the initial open-loop period.

Our study showed that the initial OFRs elicited by the *mf* and 3*f*4*f* stimuli were *always* in the direction of their principal Fourier components (i.e., the 3*f* component of the 3*f*4*f* stimulus and the 3rd harmonic of the *mf* stimulus) rather than in the direction of the overall pattern or feature. In fact, the 4*f* component of the 3*f*4*f* stimulus often had almost no impact on the monkey's initial OFR, including the temporal profiles (Fig. 4). Thus, when the R–L response measures obtained with the 3*f*4*f* stimuli were plotted in terms of the contrast of their 3*f* component, they matched the measures obtained with the pure 3*f* stimulus quite closely (except in monkey B at higher contrasts, when they fell slightly short). Similar plots of the data obtained with the *mf* stimulus—using the contrast of the 3rd harmonic rather than of the whole pattern—mimicked the plots for the 3*f* stimuli only at low contrasts and then fell progressively short with higher contrast. These data are all very similar to those obtained on humans by Sheliga et al. (2005a), further reinforcing the view that the monkey is a good animal model for the initial OFR of humans.

4.2. The initial OFR: A response to 1st-order motion energy

Sheliga et al. (2005a) argued that the dependence on the motion of the principal Fourier components of the *mf* and 3*f*4*f* stimuli—rather than on the motion of their features—indicated that the motion detectors responsible for the initial OFR in humans do not operate directly on the raw retinal images but rather on a spatially filtered version of those images, as in the well-known 1st-order energy model of motion detection that relies on oriented spatio-temporal filters: see Lu and Sperling (2001) for review. Using *mf* stimuli lacking the 5th and 7th harmonics, Sheliga et al. (2005a) were also able to show that the initial OFRs elicited by the usual *mf* stimulus fell short of those elicited by the pure 3*f* stimulus mostly because of the higher harmonics, with perhaps a very minor contribution from distortion products due to an early compressive non-linearity in the visual pathway. Thus, Sheliga et al. largely ruled out even a minor rôle for feature-based mechanisms in the genesis of the initial OFR of humans. Although we do not have data for the monkey that clarifies the role of the higher harmonics, we have demonstrated that the monkey's initial OFR shares much in common with that of the human. Further, the similarity of the contrast-dependence of the 3*f*4*f* and pure 3*f* data is consistent with mediation by oriented spatio-temporal filters as in the 1st-order motion-energy model and indicates that feature-based mechanisms make at best only a minor contribution to the monkey's OFR with this 3*f*4*f* stimulus.

Sensitivity to low-contrast stimuli (<20%), such as we here report for the monkey's OFR, is considered one of the characteristics that, in humans, sets the 1st-order motion energy mechanisms apart from feature-based mechanisms (Lu & Sperling, 1995; Nishida, 1993; Smith, 1994; Solomon & Sperling, 1994; Takeuchi & De Valois, 1997). Consistent with this, the study of O'Keefe and Movshon (1998) on monkeys showed that MT neurons have poor contrast-sensitivity for 2nd-order motion. Yet, Benson and Guo (1999) reported that the initial OFRs to a pure 2nd-order motion stimulus (defined by contrast modulated noise) were little different from those to a stimulus with strong 1st-order motion energy (except for a small latency difference, averaging ~11 ms). This observation, which was made only on a single monkey, would seem to be at odds with our findings, perhaps suggesting that some types of 2nd-order motion are much more effective in initiating OFR than others.

5. Closing remarks

Earlier studies in monkeys (Busettini, Miles, & Schwarz, 1991; Kawano & Miles, 1986; Miles et al., 1986) and humans (Busettini, Miles, Schwarz, & Carl, 1994; Gellman et al., 1990) demonstrated a number of functional similarities between the OFRs of the two species which fostered the idea that the monkey was a good animal model for the human. Our present findings on the initial OFRs elicited in monkeys by motion applied to complex grating patterns are largely in accord with the findings in a recent study on humans that used these same visual stimuli (Sheliga et al., 2005a), suggesting that the similarities between the two species extend to the detectors whereby they sense visual motion.

Acknowledgments

This work was supported by the JSPS.KAKENHI (#16GS0312), the MEXT.KAKENHI (#17700309), the Japan-US Brain Research Cooperative Program, and the Intramural Research Program of the NIH, the National Eye Institute.

References

Adelson, E. H. (1982). Some new motion illusions, and some old ones, analysed in terms of their Fourier components. *Investigative Ophthalmology & Visual Science, 34*(Suppl.), 144, Abstract.

Adelson, E. H., & Bergen, J. R. (1985). Spatiotemporal energy models for the perception of motion. *Journal of the Optical Society of America A, 2*, 284–299.

Albrecht, D. G., Geisler, W. S., Frazor, R. A., & Crane, A. M. (2002). Visual cortex neurons of monkeys and cats: Temporal dynamics of the contrast response function. *Journal of Neurophysiology, 88*, 888–913.

Albrecht, D. G., & Hamilton, D. B. (1982). Striate cortex of monkey and cat: Contrast response function. *Journal of Neurophysiology, 48*, 217–237.

Albright, T. D. (1992). Form-cue invariant motion processing in primate visual cortex. *Science, 255*, 1141–1143.

Baro, J. A., & Levinson, E. (1988). Apparent motion can be perceived between patterns with dissimilar spatial frequencies. *Vision Research, 28*, 1311–1313.

Benson, P. J., & Guo, K. (1999). Stages in motion processing revealed by the ocular following response. *Neuroreport, 10*, 3803–3807.

Brainard, D. H. (1997). The psychophysics toolbox. *Spatial Vision, 10*, 433–436.

Brown, R. O., & He, S. (2000). Visual motion of missing-fundamental patterns: motion energy versus feature correspondence. *Vision Research, 40*, 2135–2147.

Busettini, C., Miles, F. A., & Schwarz, U. (1991). Ocular responses to translation and their dependence on viewing distance. II. Motion of the scene. *Journal of Neurophysiology, 66*, 865–878.

Busettini, C., Miles, F. A., Schwarz, U., & Carl, J. R. (1994). Human ocular responses to translation of the observer and of the scene: Dependence on viewing distance. *Experimental Brain Research, 100*, 484–494.

Chen, K. J., Sheliga, B. M., Fitzgibbon, E. J., & Miles, F. A. (2005). Initial ocular following in humans depends critically on the Fourier components of the motion stimulus. *Annals of the New York Academy of Sciences, 1039*, 260–271.

Fuchs, A. F., & Robinson, D. A. (1966). A method for measuring horizontal and vertical eye movement chronically in the monkey. *Journal of Applied Physiology, 21*, 1068–1070.

Gellman, R. S., Carl, J. R., & Miles, F. A. (1990). Short latency ocular-following responses in man. *Visual Neuroscience, 5*, 107–122.

Georgeson, M. A., & Harris, M. G. (1990). The temporal range of motion sensing and motion perception. *Vision Research, 30*, 615–619.

Georgeson, M. A., & Shackleton, T. M. (1989). Monocular motion sensing, binocular motion perception. *Vision Research, 29*, 1511–1523.

Hammett, S. T., Ledgeway, T., & Smith, A. T. (1993). Transparent motion from feature- and luminance-based processes. *Vision Research, 33*, 1119–1122.

Hays, A. V., Richmond, B. J., & Optican, L. M. (1982). A UNIX-based multiple process system for real-time data acquisition and control. *WESCON Conference Proceedings, 2*, 1–10.

Heuer, H. W., & Britten, K. H. (2002). Contrast dependence of response normalization in area MT of the rhesus macaque. *Journal of Neurophysiology, 88*, 3398–3408.

Ilg, U. J., & Churan, J. (2004). Motion perception without explicit activity in areas MT and MST. *Journal of Neurophysiology, 92*, 1512–1523.

Judge, S. J., Richmond, B. J., & Chu, F. C. (1980). Implantation of magnetic search coils for measurement of eye position: An improved method. *Vision Research, 20*, 535–538.

Kawano, K., Inoue, Y., Takemura, A., Kodaka, Y., & Miles, F. A. (2000). The role of MST neurons during ocular tracking in 3D space. *International Review of Neurobiology, 44*, 49–63.

Kawano, K., & Miles, F. A. (1986). Short-latency ocular following responses of monkey. II. Dependence on a prior saccadic eye movement. *Journal of Neurophysiology, 56*, 1355–1380.

Kawano, K., Shidara, M., Watanabe, Y., & Yamane, S. (1994). Neural activity in cortical area MST of alert monkey during ocular following responses. *Journal of Neurophysiology, 71*, 2305–2324.

Kodaka, Y., Miura, K., Suehiro, K., Takemura, A., & Kawano, K. (2004). Ocular tracking of moving targets: Effects of perturbing the background. *Journal of Neurophysiology, 91*, 2474–2483.

Lu, Z. L., & Sperling, G. (1995). The functional architecture of human visual motion perception. *Vision Research, 35*, 2697–2722.

Lu, Z. L., & Sperling, G. (2001). Three-systems theory of human visual motion perception: Review and update. *Journal of the Optical Society of America A, 18*, 2331–2370.

Masson, G. S., Busettini, C., Yang, D.-S., & Miles, F. A. (2001). Short-latency ocular following in humans: Sensitivity to binocular disparity. *Vision Research, 41*, 3371–3387.

Masson, G. S., & Castet, E. (2002). Parallel motion processing for the initiation of short-latency ocular following in humans. *The Journal of Neuroscience, 22*, 5149–5163.

Masson, G. S., Yang, D. S., & Miles, F. A. (2002). Reversed short-latency ocular following. *Vision Research, 42*, 2081–2087.

Miles, F. A. (1998). The neural processing of 3-D visual information: Evidence from eye movements. *The European Journal of Neuroscience, 10*, 811–822.

Miles, F. A., Kawano, K., & Optican, L. M. (1986). Short-latency ocular following responses of monkey. I. Dependence on temporospatial properties of visual input. *Journal of Neurophysiology, 56*, 1321–1354.

Naka, K. I., & Rushton, W. A. (1966). S-potentials from colour units in the retina of fish (Cyprinidae). *Journal of Physiology, 185*, 536–555.

Nishida, S. (1993). Spatiotemporal properties of motion perception for random-check contrast modulations. *Vision Research, 33*, 633–645.

O'Keefe, L. P., & Movshon, J. A. (1998). Processing of first- and second-order motion signals by neurons in area MT of the macaque monkey. *Visual Neuroscience, 15*, 305–317.

Pantle, A., & Turano, K. (1992). Visual resolution of motion ambiguity with periodic luminance- and contrast-domain stimuli. *Vision Research, 32*, 2093–2106.

Pelli, D. G. (1997). The VideoToolbox software for visual psychophysics: Transforming numbers into movies. *Spatial Vision, 10*, 437–442.

Read, J. C., & Cumming, B. G. (2003). Testing quantitative models of binocular disparity selectivity in primary visual cortex. *Journal of Neurophysiology, 90*, 2795–2817.

Sclar, G., Maunsell, J. H., & Lennie, P. (1990). Coding of image contrast in central visual pathways of the macaque monkey. *Vision Research, 30*, 1–10.

Sheliga, B. M., Chen, K. J., Fitzgibbon, E. J., & Miles, F. A. (2005a). Initial ocular following in humans: A response to first-order motion energy. *Vision Research, 45*, 3307–3321.

Sheliga, B. M., Chen, K. J., Fitzgibbon, E. J., & Miles, F. A. (2005b). Short-latency disparity vergence in humans: Evidence for early spatial filtering. *Annals of the New York Academy of Sciences, 1039*, 252–259.

Smith, A. T. (1994). Correspondence-based and energy-based detection of second-order motion in human vision. *Journal of the Optical Society of America A, 11*, 1940–1948.

Solomon, J. A., & Sperling, G. (1994). Full-wave and half-wave rectification in second-order motion perception. *Vision Research, 34*, 2239–2257.

Takemura, A., Inoue, Y., & Kawano, K. (2002). Visually driven eye movements elicited at ultra-short latency are severely impaired by MST lesions. *Annals of the New York Academy of Sciences, 956*, 456–459.

Takeuchi, T., & De Valois, K. K. (1997). Motion-reversal reveals two motion mechanisms functioning in scotopic vision. *Vision Research, 37*, 745–755.

Yang, D. S., & Miles, F. A. (2003). Short-latency ocular following in humans is dependent on absolute (rather than relative) binocular disparity. *Vision Research, 43*, 1387–1396.